Chemistry Europe
European Chemical Societies Publishing

WILEY VCH

Excellence in Chemistry Research

Announcing our new flagship journal

- Gold Open Access
- Publishing charges waived
- Preprints welcome
- Edited by active scientists

Meet the Editors of *ChemistryEurope*

Luisa De Cola
Università degli Studi di Milano Statale, Italy

Ive Hermans
University of Wisconsin-Madison, USA

Ken Tanaka
Tokyo Institute of Technology, Japan

ChemCatChem

Research Article
doi.org/10.1002/cctc.202200477

Chemistry Europe
European Chemical Societies Publishing

www.chemcatchem.org

Nanorod Photocatalysts for C–O Cross-Coupling Reactions

Kaituo Dong,[a] Cristofer Pezzetta,[b] Qiu-Cheng Chen,[a] Alexander Kaushansky,[a] Amedeo Agosti,[c] Giacomo Bergamini,[c] Robert Davidson,*[b] and Lilac Amirav*[a]

Carbon-heteroatom cross-coupling reactions are significant for numerous industrial chemical processes, in particular for the synthesis of pharmaceuticals, agrochemicals, and biologically active compounds. Photocatalyst/transition metal dual catalytic systems pave a new avenue for organic cross-coupling reactions. Specifically, the use of semiconductor nanoparticles as heterogeneous light sensitizers is highly beneficial for industrial-scale applications owing to their low-cost production, tunable photophysical properties, facile separation, high photostability, and recyclability. Here, CdSe@CdS nanorod photocatalysts are combined with a Ni complex catalyst for the promotion of selective light-induced C–O cross-coupling reactions between aryl halides and alkyl carboxylic acids. This efficient dual photocatalytic system displays a high yield (~96%), with an impressive turnover number (TON) of over 3×10^6, and within a relatively short reaction time as a result of high turnover frequency (TOF) of ~56 s^{-1}. In addition, the nanorod photocatalysts harness light with improved solar to product efficiency compared to alternative systems, signaling towards potential solar-powered chemistry. A reaction mechanism involving energy transfer from the nanorods to the Ni complex is proposed and discussed, along with specific benefits of the seeded rod morphology.

Introduction

Since the 1970s, cross-coupling reactions have established a central role in synthetic chemistry, particularly when they are utilized for the development of natural compounds for the pharmaceutical industry, agricultural substances, optoelectronic applications and more.[1–8] Specifically, methods that facilitate carbon-heteroatom bond formation under mild conditions appeal to applications that require late-stage functionalization of sensitive synthetic targets. While forging bonds between unsaturated carbons is now considered straightforward, promoting cross-coupling with saturated centers is still challenging.[9–10] Hence, recent years have witnessed a sprout of interest in photo redox assisted catalysis. In 2014, Tellis et al.[11] and Zuo et al.[12] proposed the utilization of light-activated catalyst to enable more effective single electron reaction mechanism rather than the two-electron pathway typical to traditional protocols. Light-induced redox catalysis was proposed to facilitate redox neutrality in a traditional trans-metalation, in which single electron transfer from the light-activated catalyst to the saturated carbon effectively enhances its reactivity. In 2017, MacMillan and coworkers harnessed energy transfer from a molecular iridium sensitizer complex to stimulate an organometallic nickel catalyst to its excited state for the coupling of aryl halides with carboxylic acids.[13] This approach relies on molecular sensitizers to efficiently absorb light and then transfer the energy to a transition metal catalytic compound to spur its reactivity. Hence, it appears the adopted photocatalysts may either oxidize the organometallic complex into a higher unstable metal state, or transfer energy to excite the organometallic complex, in order to switch on the reductive elimination reaction.[9,10,13,14] Regardless of the exact mechanism, photosensitizer/Ni dual catalysis has drawn significant attention due to the high efficacy and mild reaction conditions it requires.

Most recently, dual catalysis using heterogeneous photosensitizers for C-heteroatom bond formation was proposed as a viable and attractive alternative, with particular appeal to the industry due to the relatively lower price of heterogeneous catalysts, recycling possibilities, and potential for easier scale-up for mass production.[15,16] With well-matched band edge positions, cadmium chalcogenides are of particular appeal for serving as the visible light sensitizer component in such schemas.[17] With an inspiring work, Krauss, Weix and coworkers reported on utilizing CdSe quantum dots as efficient photocatalysts for carbon-carbon bond formation that may also extend to carbon-nitrogen coupling.[18] Recently, Liu et al. successfully demonstrated the feasibility of a heterogeneous catalytic strategy for C–N and C–O coupling reactions of aryl halides with amines and alcohols using CdS quantum dots as the light sensitizer component.[19] Indeed, semiconductor nanocrystals are particularly advantageous as photosensitizers thanks to their photostability, high molar extinction coefficients,

[a] Dr. K. Dong, Dr. Q.-C. Chen, Dr. A. Kaushansky, Prof. L. Amirav
Schulich Faculty of Chemistry
Technion–Israel Institute of Technology
32000 Haifa (Israel)
E-mail: lilac@technion.ac.il
[b] Dr. C. Pezzetta, Dr. R. Davidson
Dr. Reddy's Laboratories (EU) Ltd
410 Science Park, Milton Road, CB4 0PE Cambridge (United Kingdom)
E-mail: rob.w.davidson@gmail.com
[c] Dr. A. Agosti, Prof. G. Bergamini
Chemistry Department "Giacomo Ciamician"
University of Bologna
40129 Bologna (Italy)

Supporting information for this article is available on the WWW under https://doi.org/10.1002/cctc.202200477

and the ease in which their electronic and photophysical properties may be tuned based on size and shape.[20] Yet, the utilization of colloidal quantum nanocrystals for the promotion of organic transformations is still embryonic. Hence, many open questions remain with regards to the underlying mechanism, and the reaction efficiency in terms of both turnover number and light-harvesting still calls for improvements.

Here we utilized a well-controlled nanoscale structure consisting of a cadmium selenide (CdSe) quantum dot that is embedded asymmetrically within a cadmium sulfide (CdS) quantum rod.[21–24] The light absorption and charge separation events in this colloidal CdSe@CdS nanorod system can be tuned by variations of the dot diameter and the rod length.[25,26] The seeded rod (SR) morphology has several distinguishing characteristics. Foremost is the system's strong absorption of light, including in the visible range, which is accompanied by very high photoluminescence quantum yield. Furthermore, since electrons are delocalized throughout the CdS rod, while holes are three-dimensionally confined to the CdSe quantum dot, the SR are characterized by an extended excited state lifetime. These properties indicate high potential for supporting applications that call for energy transfer. In addition, SRs are also highly compelling for applications that require charge transfer since the rods can be tipped with a metal domain in order to further minimize charge recombination. Highly efficient oxidative activity of such system was demonstrated for the oxidization of OH^- to OH radical,[27] and for the endothermic oxidation of benzylamine, alongside efficient production of H_2.[28] Given that photocatalytic C–O cross-coupling reactions may be governed either by charge or energy transfer, the selection of a system such as SR that can potentially facilitate both pathways is highly beneficial. Herein, the SR served as heterogeneous photosensitizers, facilitating energy transfer to excite a molecular Ni catalyst. The dual system was successfully employed for efficient and selective cross-coupling reactions between alkyl carboxylic acids and aryl halides. The esterification coupling was realized with significantly lower catalyst loading and shorter reaction duration in comparison to dominant literature reports, making it highly appealing for industrial applications. Optimization conditions and reaction mechanisms are discussed.

Results and Discussion

The CdSe@CdS nanorod heterogeneous photocatalysts (Figure 1) are synthesized via classical colloidal chemistry following an established protocol. Since the activity of any given photocatalytic reaction is strongly influenced by the rod's morphology, throughout the course of this research, the utilized rods were 40 nm long, 4.3 nm wide, and with 2.3 nm CdSe seed size. The reader is referred to the supporting information section for full account of the synthesis protocols, and optical and structural characterization of the SR (Figures S1–2). The absorption spectrum of the investigated SR (Figure S2B) shows the characteristic absorption features of the lowest exciton transition (between the valence band edge and the lowest conduction band level) that is localized in the CdSe seed

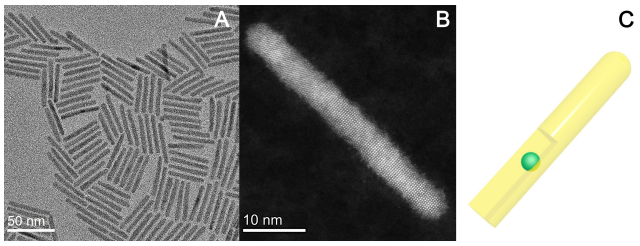

Figure 1. SRs visualized with (A) TEM image, (B) HAADF-STEM image of a single SR with high resolution, (C) illustration of the rod depicting the embedded seed.

(563 nm). In addition, features at 462 and 422 nm are clearly seen, and are ascribed to the CdS rod 1Σ ($1\sigma e-1\sigma h$) and 1Π ($1\pi e-1\pi h$) exciton transitions, respectively. These transitions relate to discrete band levels due to quantum confinement of the CdS in the radial direction. The spectrally narrow photoluminescence (27.5 nm full width at half maximum) with an emission peak at 575 nm (2.15 eV), testifies of the rods high quality (Figure S2B).

A wide parameter field was examined in the search for optimized reaction conditions, including the proper selection of Ni salt and its amount, reaction duration, illumination intensity, excitation wavelength, solvent type and amount, and modifications to the SR (Table S1, Figure S3, Table S8, Table 1). In the standard / optimized protocol, a small amount of SR photocatalysts (0.62 mg, $2.7*10^{-7}$ mmol, which account for $0.27*10^{-3}$ mol% compared with the aryl halide substrate, dispersed in 0.2 mL toluene) was added to a glass vial together with 2 mL dimethylformamide (DMF, to obtain a final rods concentration of 0.3 mg/mL), and 0.1 mmol methyl 4-bromobenzoate (1 equiv.) as aryl halide substrate, 0.15 mmol Boc-L-proline (Boc-Pro-OH) as alkyl carboxylic acid substrate, 30 mol% nickel(II) chloride ethylene glycol dimethyl ether complex ($NiCl_2 \cdot DME$) as the transition-metal catalyst, 45 mol% 4,4′-Di-

Table 1. Establishing essential conditions for the C–O cross-coupling reaction.

Entry	Condition	1 [%][b]	2 [%][b]	3 [%][b]	Halide substrate [%]
1	Standard[a]	96[c]	0	0	0
2	Dark (room temperature)	0	0	0	98
3	Dark (40 °C)	0	0	0	93
4	No SR	0	0	0	89
5	No $NiCl_2 \cdot DME$	< 0.01	0	0	93.5
6	No dtbbpy	< 0.01	0	0.5	85
7	No base	0	0	0	85
8	Excitation at 565 nm 200 mW	25	0	0	65.5

[a] Reaction conditions: methyl 4-bromobenzoate (0.1 mmol), Boc-Pro-OH (0.15 mmol), SR (0.62 mg, $2.7*10^{-7}$ mmol), $NiCl_2 \cdot DME$ (0.03 mmol), dtbbpy (0.045 mmol), Cs_2CO_3 (0.15 mmol), DMF (2 mL, anhydrous), 455 nm LEDs with 300 mW at 40 °C. [b] Calculated by ^{1}H-NMR using 0.1 mmol 1,3,5-trimethoxybenzene as internal standard. [c] Isolated yield for the standard experiment ~83%.

tert-butyl-2,2′-bipyridine (dtbbpy) as the ligand which will coordinate to the Ni^{2+} ion to form a Ni complex, and 1.5 equiv. Cs_2CO_3 as base to facilitate the deprotonation of alkyl carboxylic acid. The reader is referred to the supporting information for further details. The solution was then illuminated using a 455 nm LED operating at 300 mW for a duration of 9 hours (Scheme 1). At the end of the reaction, the organic product was extracted in methyl tert-butyl ether and washed with brine. The reaction yield was determined via ^{1}H-NMR analysis employing 1,3,5-trimethoxybenzene as internal standard.

These conditions resulted in a reaction yield of ~96% for C–O cross-coupling between methyl 4-bromobenzoate and alkyl carboxylic acid (Boc-Pro-OH), with high selectivity towards product **1** (Scheme 1). Significantly, temporal dependence of conversion efficiency [Figure S3 B] shows it to complete within merely 9 hr, half the reaction duration reported for the $Ir(ppy)_3$/Ni dual system.[13] Prolonged irradiation (132 hr) was found to jeopardize the product, as only 47% was recovered.

Various solvents, Ni salts, ligands for the Ni catalyst complex, and bases were also examined. It was found that among the solvents tested, DMF with its medium polarity resulted with the best performance (Table S2). $NiCl_2 \cdot DME$, which has the simplest anionic counterpart, provided the best results among Ni salts that were tested (Table S3). In general, ligands containing bipyridine moieties outperformed those with phenanthroline moieties, and among the bipyridines, dtbbpy afforded the best reaction yield (Table S4). Utilization of the very similar ligand 4,4′-Dimethyl-2,2′-bipyridyl resulted with 70% efficiency.

In order to verify the light-induced nature of the reaction and determine the role each component plays, a set of control experiments was conducted, as detailed in Table 1. It is confirmed that the C–O cross-coupling reaction does not occur in the absence of an illumination source (at ambient or slightly elevated temperatures), or without the presence of SR photocatalysts and Ni complex (i.e., Ni salt, ligand, and the based which is required to enable the complex formation).

For the conditions shown, the reaction yield showed dependency on the light intensity in the reactor configuration used, with yields gradually increasing from 31% to 49% and 96% when the LED power was raised from 100 mW to 200 mW and finally 300 mW (Figure S3 C), further confirming a light-induced mechanism. Hence 300 mW was selected as the optimal excitation intensity for establishing the substrate scope.

Once optimized reaction conditions were identified, we began exploring the scope of reactions between various aryl halides (Figure 2 in blue) and carboxylic acids (Figure 2 in red) that can be promoted using the dual system of molecular Ni catalyst and SR. As shown in Figure 2, the SR heterogeneous photocatalytic system successfully supported reactions between alkyl carboxylic acids and a diverse array of electron-deficient aryl bromides or iodides, with a variety of functional groups spanning from trifluoromethyl (**5**), ester (**6**), aldehyde (**7**), ketone (**8**), to nitrile (**9**). Unless specified, all reactions were performed under the aforementioned 'standard' optimized conditions.

Aryl iodides outperformed the respective aryl bromides in the presence of a *para*-trifluoromethyl group (products **5**), and displayed comparable activity with aldehyde, ketone, and nitrile groups (products **7**, **8**, **9**). Yet, for aryl halides with an ester group, the final yield obtained with the aryl bromide substrate was higher than that obtained with the iodinated analog (product **6**). For the dihalide-benzene substrates, 4-bromo/iodo/fluoro-bromobenzene were adopted, and the iodo group reacted preferentially to achieve 80% yield (product **10**), much higher than that with the bromo group (46%). 4-Fluorobromobenzene only afforded 2% yield (product **14**); with 4-fluoroiodobenzene a 8% yield was obtained instead, comparing well against the lack of reactivity reported when C_3N_4 was adopted.[15] When these di-halide substrates were used, the expected di-ester product was not found, suggesting that the esterification product deactivated the aryl bromide component towards a second esterification. Some electron-neutral and electron-rich aryl bromides (bromobenzene, 4-bromotoluene) (**22**, **23**) did not react, while 4-bromobiphenyl afforded C–O product **13** in 27% yield within 9 hours. Therefore, besides electron-deficient substrates (products **5**–**10**), our reaction system could be extended to some electron-rich aryl bromide substrates for C–O cross-coupling. The reaction of *ortho*-substituted aryl bromides also afforded products **11** and **12** in 36% and 15% yield, respectively, lower than the corresponding *para*-substituted derivatives, suggesting steric effects might hinder the cross-coupling reaction. These yields, however, are significantly better than those obtained using C_3N_4 as photocatalyst.[15]

Considering the carboxylic acid counterpart, different substrates can be efficiently coupled with the selected aryl halide. These include aliphatic (**15**, **21**), benzoic (**16**, **18**), and olefinic (**17**) acids. It appears that some of the reactions follow slower kinetics, and thus require longer illumination time, as can be seen for **16** and **17**, for which 36 hours of continuous illumination improved the reaction yield. Proline protected with Boc or Cbz groups was found to support high reaction yields of over 80% (products **19**, **6**). However, when pure Proline (**23**) was examined as substrate, the expected C–O coupling product was not found. Pleasingly, when pyrrolidine was tested as a

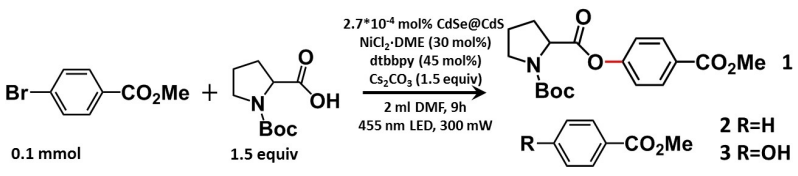

Scheme 1. The standard/optimized protocol for cross-coupling reactions between alkyl carboxylic acids and aryl halides with a dual system of molecular Ni catalyst and SR as heterogeneous photosensitizers.

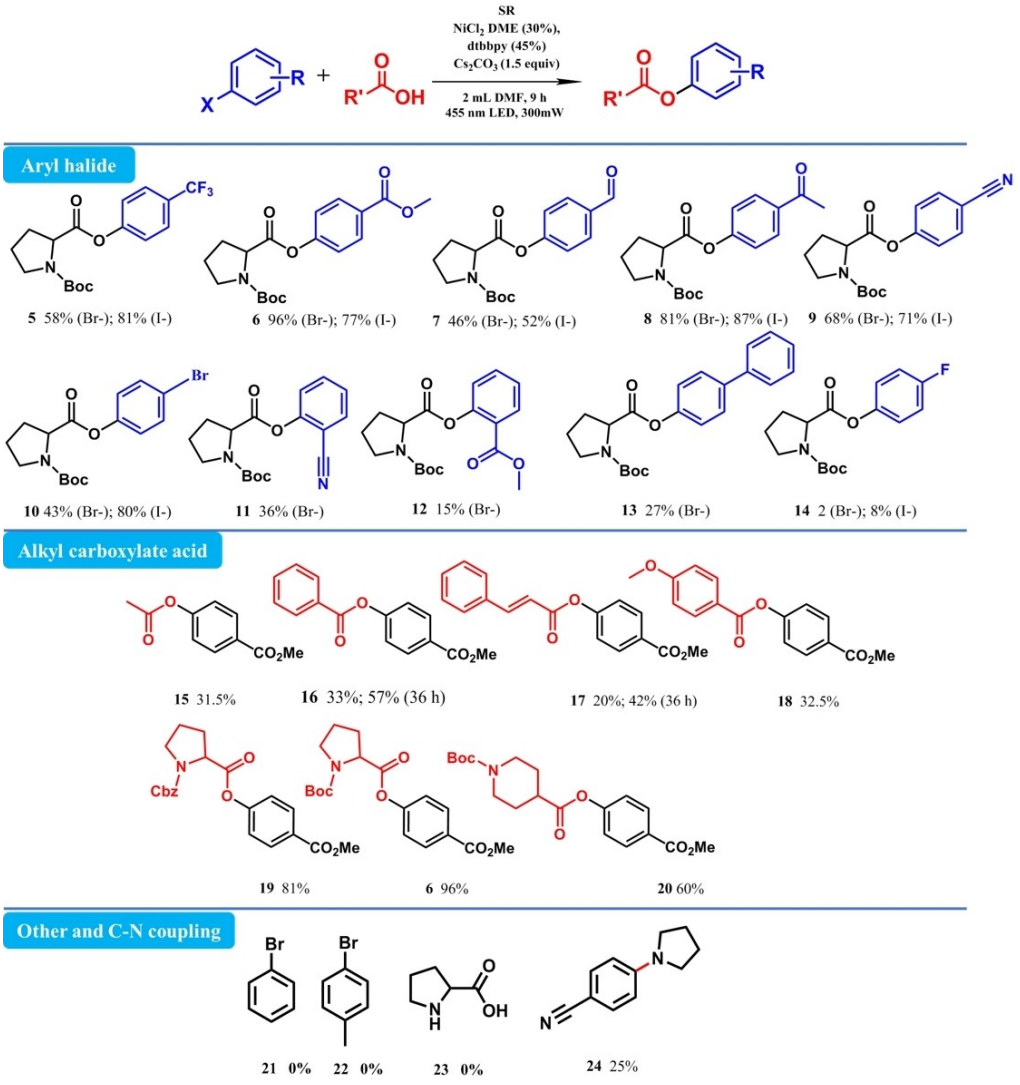

Figure 2. Scope of SR-assistant photocatalytic C–O cross-coupling between alkyl carboxylic acids and aryl halides. Reaction conditions: methyl 4-bromobenzoate (0.1 mmol), Boc-Pro-OH (0.15 mmol), SR (0.62 mg, $2.7*10^{-7}$ mmol), $NiCl_2 \cdot DME$ (0.03 mmol), dtbbpy (0.045 mmol), Cs_2CO_3 (0.15 mmol), DMF (2 mL, anhydrous), 455 nm LEDs with 300 mW at 40 °C. The yield is calculated by ^{1}H-NMR using 0.1 mmol 1,3,5-trimethoxybenzene as internal standard.

coupling partner, an alternative C–N cross-coupling reaction pathway was observed, and 25% yield of product **24** was obtained. This clearly testifies to the great potential of the SR-based dual photocatalytic system and indicates further possibilities that will call for follow-up research.

One of the key advantages of heterogeneous photocatalysis is the possibility to recycle and reuse the catalyst. To demonstrate this, cyclic tests were performed, in which the SR were recovered (i.e., separated, collected, and washed) at the end of each reaction by simple and straightforward centrifugation, and were reused once more for another reaction cycle (with fresh Ni catalyst). As can be seen in Figure 3, after a mild initial drop in yield for **1** that follows the first cycle, the photocatalytic system maintains consistent activity within 10 cycles. These results clearly demonstrate the compelling reusability of SR.

Given the interest in the progression towards industrial applicability, reaction throughput was further investigated (specifically the amount of substrate that can be reacted using a given amount of photocatalyst). Turnover number (TON) for the SR photocatalytic system was calculated as the molar ratio between the C–O products that are detected and the rods (detailed description of the calculation is provided in the SI). Table 2 summarizes our findings regarding efficiency and TON dependency on substrate amount, while using a fixed amount of SR, Ni salt, and ligands. The latters were held as per the chosen standard conditions, while substrates and base amounts were changed in the range of 2–16 folds. The substrate concentration was kept as 0.1 mmol/mL.

It was found that 4-fold the amount of substrate still reacts at a relatively unaffected high yield. In addition, moderately high yields of 60–70% can be obtained even for 8 to 16-fold increase in substrate amount, though a longer reaction duration

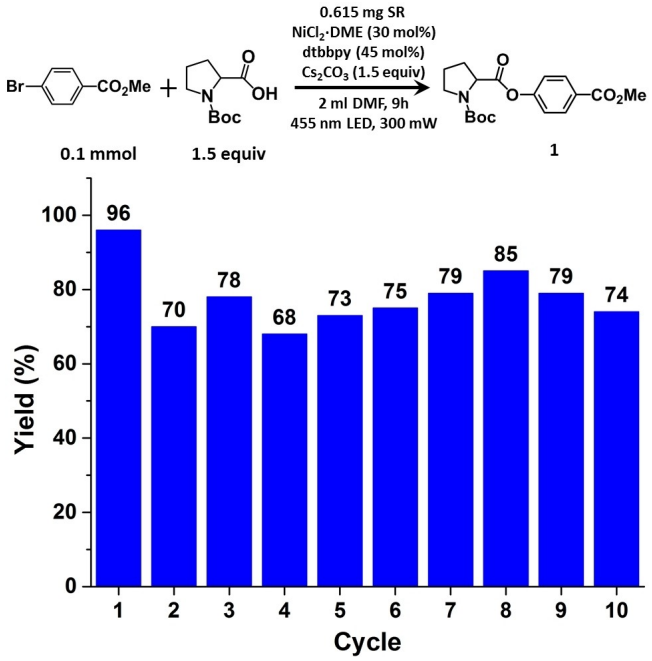

Figure 3. Cyclic performance of SR for C–O cross-coupling between alkyl carboxylic acid and aryl halide. The yield is calculated by ^{1}H-NMR using 0.1 mmol 1,3,5-trimethoxybenzene as internal standard.

is required. To some extent this may be regarded as an alternative to recycling of the photocatalytic rods, with the exclusion of separation and washing steps.

An impressive TON of 3.62*10^6 was achieved and likely may be further improved given that the SRs are still active and may be recycled again. Since most heterogeneous photocatalytic systems are not based on individual particles that offer a single well-defined catalytic site, their activity is typically quantified per unit of mass rather than molar ratio as in the TON definition. In that context, and of significance, is the relatively low amount of photocatalyst that is required here to support the catalytic reaction, or conversely, the impressively high amount of aryl halide that is converted per mg of SR. For comparison, using C_3N_4 the Pieber group reports a conversion of 0.03 mmol aryl halide per mg photocatalyst, and the MacMillan group reports on the conversion of 0.15 mmol aryl halide per mg of $Ir(ppy)_3$ photocatalyst.[13,15] Herein, we report on successful catalytic conversion of 2.6 mmol aryl halide per mg of SR, nearly two orders of magnitude higher than that obtained with C_3N_4 [see Table S6 for more information]. The high efficiency and significant TON, and the possibility to utilize a minimal amount of SR to convert a large amount of substrate, demonstrate the superior catalytic performance of the SR system in comparison with other established photocatalysts.

For industrial applications the turnover frequency is another important aspect to be considered. It is essentially defined as the number of generated products per second (unit of time) per catalytic site, and in this case equal to the TON divided by reaction time. The impressive TON of 3.62*10^6 was achieved following 18 hr of reaction, resulting with TOF of ~56 sec^{-1}, or 200,000 hr^{-1}. Simply put, 56 molecules of aryl halide are converted every second (200,000 per hr) on every rod to form the new C–O bond. For comparison, with a world record nearly perfect photon to H_2 conversion efficiency, Pt tipped SR produced H_2 with TOF of 360,000 molecules per hour per rod.[27] Examination of data from Krauss-Weix implies that their CdSe QDs supported a TOF of ~10 cross-coupling reactions per dot per sec (36,000 per hr).[18] Given that the reaction here is light-induced, and the photon flux plays a critical role in directing and dictating the reaction's efficiency and kinetics, the improved TOF of the SR system in comparison with the dots might be attributed to the stronger molar extinction coefficient (10^6~10^7 M^{-1}·cm^{-1} for SR vs. ~10^5 M^{-1}·cm^{-1} for dots).[24,29,30]

Lastly, as this is a photocatalytic reaction, and given the clear motivation to transition towards solar-powered chemistry, the efficiency of photon-to-product conversion (QE) is also of interest. Here a maximum efficiency of 1.3% was attained. While this still leaves room for improvement, it is already nearly an

Table 2. Scale-up experiments of substrate to SR ratio.

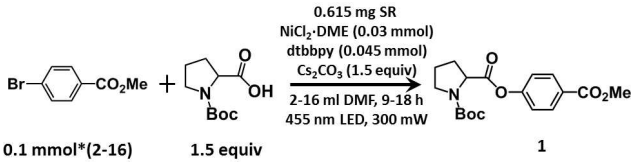

Entry		Methyl 4-bromobenzoate (mmol)	Boc-Pro-OH (mmol)	Cs_2CO_3 (mmol)	DMF (mL)	Efficiency[b]	TON
1	One portion[a]	0.1	0.15	0.15	2	96%	3.56*10^5
2	2-folds	0.2	0.3	0.3	2	77.5%	5.75*10^5
3	4-folds	0.4	0.6	0.6	4	89.2%	1.32*10^6
4	6-folds	0.6	0.9	0.9	6	49%	1.09*10^6
5	8-folds	0.8	1.2	1.2	8	46.1%	1.37*10^6
6	8-folds	0.8	1.2	1.2	8	71% (18 h)	2.11*10^6
7	16-folds	1.6	2.4	2.4	16	61% (18 h)	3.62*10^6

Note: Molar ratio, SR rods number: substrate (0.1 mmol methyl 4-bromobenzoate), 1: 3.706*10^5.
[a] Reaction conditions: methyl 4-bromobenzoate (0.1 mmol), Boc-Pro-OH (0.15 mmol), SR (0.62 mg, 2.7*10^{-7} mmol), $NiCl_2$·DME (0.03 mmol), dtbbpy (0.045 mmol), Cs_2CO_3 (0.15 mmol), DMF (2 mL, anhydrous), 455 nm LEDs with 300 mW at 40 °C. [b] The efficiency was defined as the ratio of C–O product and substrate methyl 4-bromobenzoate, calculated by ^{1}H-NMR using 0.1 mmol 1,3,5-trimethoxybenzene as internal standard.

order of magnitude better than the ~0.19% that was reported for CdSe QDs.[18]

Reaction Mechanism. Unambiguous mechanistic description is a prerequisite for proper optimization strategy. Photocatalytic C–O cross-coupling reactions between aryl halide and alkyl carboxylic acid are known to progress following either a single electron transfer (SET) pathway or energy transfer pathway.[13,14] In order to ascertain the dominant reaction mechanism in this work we compared the activity of SR to that of metal-tipped SR. It is well established in the literature that when the SRs are tipped with a metal nanoparticle such as Pt or Ni (Top of Table 3, B – Pt-tips, and C – Ni-tips), most of the photoinduced electrons transfer into the metal domain,[31,32] while the holes localize within the CdSe core (as schematically illustrated in Figure A of Table 3).[33,34] This spatial charge separation results with significantly long lived charge separation, which is expected to be highly beneficial to processes involving direct charge transfer.[27] In contrast, such dissociation of the exciton (Figure S4) is expected to be detrimental for those processes that rely on energy transfer.

Both Pt and Ni tipped SR were adopted for the cross-coupling reactions, with results summarized in Table 3. As was already established earlier, no conversion was obtained in the absence of the Ni salt (Table 3, Entry **4**, **6**). Hence, a reaction that is initiated via direct charge transfer from the rods to the substrate may be ruled out. Of significance is the fact that the yield of the cross-coupling reaction dropped from 96% to merely 16–18% upon metal tipping of the rods, and regardless of the metal type (Entry **3**, **5**). It should be noted that all samples of tipped rods contain some population of non-tipped rods (about 5% in this case), and these may contribute to the activity, which in that case is artificially shifted to higher values. These results in which improved and long-lasting charge separation leads to lower yield for the photocatalytic cross-coupling reaction strongly support an energy transfer pathway.

Noteworthy is the fact that no Ni deposition was found to occur on the SR, even following 132 hr of reaction, as evident from HR-STEM (Figure S5). This testifies, albeit indirectly, of the stability of the SR system. Ni deposition was previously reported to occur as an unwanted side reaction during illumination of C_3N_4 in the presence of Ni salt,[15] and could be detrimental for an energy transfer process.

As shown in Table 4, when SRs were not introduced, no C–O product was detected after 9 hours of irradiation (Entry **2**). Noteworthy is the fact that C–O product was observed, with a reaction yield of approximately 50%, when the irradiation time was extended to 132 hours (Entry **3**). In addition, no unreacted halide substrate remained, indicating that the yield is capped by this value. This suggests that direct photosensitization of the Ni-complex is accessible, though significantly slower and ineffective compared with sensitization by the SR.[13]

Energy transfer from nanorods to Ni complex. For the iridium/nickel metallophotocatalysis C–O cross-coupling reaction, a triplet-triplet energy transfer mechanism was proposed.[13,14] Indeed, unpaired triplet states are known to play a significant role in a variety of reactions. Since direct photoexcitation from singlet to triplet state is inefficient, triplet states are often populated through energy transfer from a sensitizer. Recently it was demonstrated that CdSe nanoparticles might also serve as triplet sensitizers,[35] and an interfacial Dexter-like triplet-triplet energy transfer mechanism was proposed. In fact, it was proposed that nanoparticles are effective surrogates for molecular triplets due to the ill-defined spin quantum numbers and closely spaced excited-state energy levels that help circumvent the inherently large singlet-triplet energy gaps, which are typical of molecular sensitizers.[32,36,37]

In order to determine if such transfer mechanism is a viable possibility herein, the triplet energy state of the Ni complex (Figure S6A) was calculated via density functional theory (DFT). To simplify the calculation, the ligand 4,4′-dimethyl-2,2′-bipyr-

Table 3. Pt-SR and Ni-SR as photosensitizers for C–O cross-coupling.

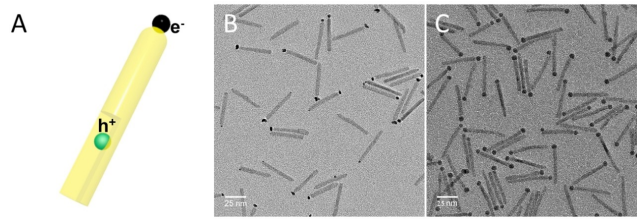

Entry	Sample	Ni salt	1 [%][b]	2 [%][b]	3 [%][b]	Halide substrate [%][b]
1	SR[a]	yes	96	0	0	0
2	No SR	yes	0	0	0	89
3	Pt-SR	yes	16	2	0	67
4	Pt-SR	no	0	0	0	100
5	Ni-SR	yes	18	1.5	0	66
6	Ni-SR	no	1	2.5	0	87

[a] Reaction conditions: methyl 4-bromobenzoate (0.1 mmol), Boc-Pro-OH (0.15 mmol), SR (0.62 mg, $2.7*10^{-7}$ mmol), $NiCl_2$·DME (0.03 mmol), dtbbpy (0.045 mmol), Cs_2CO_3 (0.15 mmol), DMF (2 mL, anhydrous), 455 nm LEDs with 300 mW at 40 °C. [b] Calculated by ^{1}H-NMR using 0.1 mmol 1,3,5-trimethoxybenzene as internal standard.

Table 4. Control of 132 hours illumination.

Entry	Conditions	Irradiation time	1 [%][b]	2 [%][b]	3 [%][b]	Halide substrate [%][b]
1	SR (standard)[a]	9 h	96	1.5	0	0
2	No SR	9 h	0	0	0	89
3	No SR	132 h	52	2	0	0
4	No SR/Ni salt	132 h	0	3.5	0	75
5	No SR/ Boc-Pro-OH	132 h	0	15	0	80

[a] Reaction conditions: methyl 4-bromobenzoate (0.1 mmol), Boc-Pro-OH (0.15 mmol), SR (0.62 mg, $2.7*10^{-7}$ mmol), $NiCl_2$·DME (0.03 mmol), dtbbpy (0.045 mmol), Cs_2CO_3 (0.15 mmol), DMF (2 mL, anhydrous), 455 nm LEDs with 300 mW at 40 °C. [b] Calculated by ^{1}H-NMR using 0.1 mmol 1,3,5-trimethoxybenzene as internal standard.

idyl was selected for the Ni complex (Figure S6B), instead of dtbbpy. This replacement is expected to have only minor effects on the final calculation result, as evident by the comparable reaction yield which was obtained using this ligand (70%, Table S4). After vertical excitation and geometry relaxation (see supporting information), the triplet-singlet energy gap was determined to be 0.897 eV when solvated in dimethylformamide, or 0.844 eV in gas phase (Figure S8A). The influence of the media can be drastic and accounting for it might be important for reliably reproducing experimental results by calculations. Since condensed phase calculations may depend on the applied solvation model, gas phase calculations are added as a reference and methodology control. Both of the calculated values are significantly low in comparison with triplet excitons that may be derived from the SR excited states (2.15 eV for the CdSe core, based on SR PL). Hence, the SRs are potentially capable of supporting exothermic energy transfer and sensitization of the Ni complex triplet state (Figure S8B).

Energy transfer pathways, in which the Ni complex excited state(s) are accessed via photosensitization (here by excited SR), may involve Förster or Dexter type mechanism.[13,14,38,39] Determining which type of energy transfer mechanism governing the reaction is vital for proper optimization. Förster energy transfer requires spectral overlap between the emission spectrum of the donor and the absorption spectrum of the accepter.[39] The absorption spectrum of the Ni-complex was calculated by Gaussian (Revision D.01)[40] using Tamm-Dancoff-approximated time-dependent DFT (TDA-DFT)[41,42] calculations by the functional: PBE0.[43] The obtained spectrum, which is shown in Figure S8C, shows no spectra overlap with the SR's photoluminescence spectra. Hence, the Förster energy transfer mechanism can be excluded.

Dexter energy transfer mechanism is based on orbital overlap between donor and acceptor, or intimate physical contact. Though the SR surfaced is covered with capping ligands (that are inherent to colloidal synthesis), this ligand shell dictates a distance of ~1.2 nm (See supporting information, section 'synthesis protocol', Figures S9–10), which is not expected to hinder energy transfer.[39] At times, the Ni complex might displace some of the capping ligands, or penetrate the shell, as the surface covering is not dense. Noteworthy is the observation of Mongin et al.,[35] which also report on triplet energy transfer from surface acceptors to freely diffusing molecular solutes. To further examine the possibility of the Dexter energy transfer mechanism, we examined the reaction yield dependence on the concentration of the Ni complex. The yield dropped to 75% and 56% upon lowering the Ni salt concentration from 0.03 mmol to 0.02 mmol and 0.01 mmol, cooperating a distance sensitive model.

The surface ligands of colloidal nanocrystals are well known for their potential to greatly influence the extraction of triplet excitons in semiconductor nanocrystals.[35,44,45] Weiss et al. tuned the composition of CdS dot's ligand shell to enhance the rate of the carbon-carbon coupling reaction.[46] Herein, the original hydrophobic surface ligands, octadecyl phosphonic acid (ODPA)/ trioctylphosphine oxide (TOPO), supported ~96% yield for the C–O cross-coupling reaction. Altering the ligand to the hydrophilic 11-mercaptoundecanoic acid (MUA) resulted with a sharp drop of the final yield to half (47%) of that obtained with the native ODPA/TOPO shell (Table S8), and 38% of halide substrate was dehalogenated and converted to the corresponding phenol.

Interestingly, when the ligand 9-anthracenecarboxylic acid (ACA) was anchored to the surface of the SR, the cross-coupling yield decreased to 30%, less than 1/3 of the original yield when ODPA/TOPO are used (Table S8, Entry **3**). ACA has been reported to be an excellent triplet exciton acceptor.[35,45] Therefore, it is stipulated that ACA effectively harnesses the excited state energy from the SR photocatalysts, thus hindering the necessary transfer to the Ni-complex. These findings further support a direct triplet energy transfer mechanism from nanorods to Ni complex.

In addition to triplet-triplet energy transfer, a singlet energy transfer is also plausible, given the bandgap of the SR with respect to the S_0-S_1 gap of Ni-complex (Figure S2 and Table S7). Yet, considering the much shorter lifetime of singlet state in nanocrystals (~10 ns), compared with the long-lived triplet energy state (~100–200 ns),[47] the possibility of singlet-singlet energy transfer is less likely to dominate the energy transfer process.

The proposed catalytic cycle is initiated with oxidative addition of aryl bromide onto Ni(0) (which originates from an in situ reductions of the initial Ni(II) complex, as described in Figure S7).[48,49] Next, an alkyl carboxylate acid coordinates with the Ni ion, thereby replacing the Br^- ion, which results with the formation of a Ni complex with the two selected substrates. Next, this metal-complex is excited to its triplet state via energy transfer from an excited SR photosensitizer. This enables the reductive elimination reaction, resulting in turnover of the Ni complex to its original oxidation state and the formation of C–O cross-coupling reaction between the two substrates (Figure 4).

The SR photocatalytic system was compared with closely related alternative colloidal semiconductor nanocrystals that may serve as sensitizers: CdS nanorods (without the CdSe seed), and CdSe dots, i.e., the two components from which the system is made. Utilizing non-seeded CdS rods resulted with a mild decrease in the reaction yield (from 96% to 70%, under the same conditions). This is expected given the lower absorption cross section of the CdS rods and the shorted exciton lifetime.[29] Surprisingly, the photocatalytic C–O cross-coupling reaction did not proceed at all when CdSe dots were examined as the light sensitizer component. Regardless of the dots amount, or which surface ligand was used, no product was detected. This can be attributed to either energetic or morphological aspects or a combination of both. First, one should note the energetic difference between CdSe and CdS, with bulk band gaps of ~1.7 eV and 2.4 eV, respectively. Yet, this is somewhat surprising, considering that CdSe should theoretically be able to support energy transfer to the Ni complex, based on its DFT calculated triplet energy state. Triplet energy transfer from quantum dots to molecule acceptors is a fascinating and complex subject that merits further research.[50] The energy transfer may be mediated by either electron or hole, which have significantly different transfer rates.[44,51] As a result, Dexter energy transfer processes were found to require specific band alignment between the nanocrystal photosensitizer and the

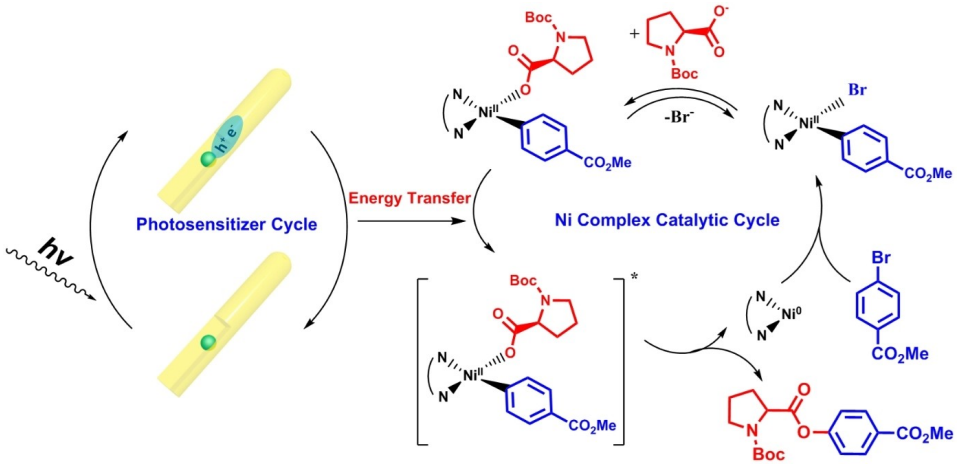

Figure 4. The proposed catalytic cycle for C–O cross-coupling between alkyl carboxylic acid and aryl bromide. The Ni complex cycle mechanism is adapted from reference 13.

molecule acceptor.[44,51,52] Therefore, beyond pure energetic criteria, the band alignment between the CdSe dots and the Ni-complex may not be favorable for the Dexter triplet energy transfer process. This hypothesis was supported with the examination of CdS dots as the light sensitizer component, which resulted with a reaction yield of 62.5%. An interesting additional aspect to consider relates to the rod morphology, which offers more opportunities for the Ni complex to interact with the semiconductor's surface in order to facilitate a Dexter-like energy transfer mechanism. This is corroborated by the ability of the seeded rods to promote a reaction, though at a lower yield, even under illumination with 565 nm LED (at 200 mW) that selectively excites the CdSe seed within the rods (Table 1, Entry 8). Hence, it is suggested that the rods morphology plays a significant role in facilitating the cross-coupling reaction.

Interestingly, CdSe dots were previously reported to support C–C cross-coupling reactions for β-alkylation, β-aminoalkylation, dehalogenation, amine arylation, and decarboxylative radical formation,[18] and yet were found here to be non-active for C–O cross-coupling between carboxylate acid and aryl halide. This might be attributed to the different underlying mechanisms. Whereas the C–O cross-coupling herein is induced via energy transfer, the C–C reactions between carboxylate acid and aryl halide were based on the charge transfer process, in which decarboxylation via photogenerated hole oxidation is necessary.[12,13]

Conclusion

Herein, CdSe@CdS nanorods were utilized successfully as light sensitizers in a heterogeneous dual photocatalytic system, together with a Ni complex catalyst. This unique combination promoted selective C–O cross-coupling reaction between a wide scope of alkyl carboxylic acids and aryl halides, with up to 96% yield, an impressive TON of $\sim 3.6\times10^6$, and a fast TOF of $\sim 56\ sec^{-1}$. These improvements are expected to be highly beneficial for industrial-scale applications. Further, the ability of such nanorod photocatalysts to harness sunlight with improved solar to product efficiency compared to alternative systems signals towards potential solar powered chemistry. Based on a set of control experiments coupled with DFT calculations, a reaction mechanism involving Dexter triplet energy transfer from the nanorods to the Ni complex is proposed. The CdSe@CdS nanorods are compared to CdSe, and CdS dots, as well as CdS rods, and the specific benefits of the seeded rod morphology are discussed. As such, this work represents an essential milestone in the development of the promising yet embryonic arena that harnesses colloidal quantum nanocrystals for the promotion of organic transformations.

Experimental Section

Synthetic Protocol

Materials: Unless otherwise indicated, starting materials were obtained from Sigma-Aldrich, Acros Co. Ltd. Important chemicals and purity are listed here: CdO, 99.99%; Trioctylphosphine (TOP), min 97%, Strem Chemicals INC.; Trioctylphosphine oxide (TOPO), 99%, Aldrich; n-octadecylphosphonic acid, Carl Roth GmbH + Co. KG; Oleylamine, 80–90%, Acros; oleic acid, 70%, Fisher Scientific UK Limited; propylphosphonic acid (PPA), Chem Cruz; Platinum(II) acetylacetonate ($Pt(AcAc)_2$), 98%, Acros; $AuCl_3$, 99.99%, Acros; octylamine, 99+%, Acros; nonanoic acid, 97%, Alfa Aesar; 1,2-hexadecaneiol, 90%; diphenyl ether, 99%. PLC Silica gel 60 F254 (0.5 mm thickness), Merck KGaA * 64271 Darmstadt * Germany.

Synthesis protocol of CdSe quantum dot seed:[27] In detail, 0.06 g CdO, 0.28 g octadecyl phosphonic acid (ODPA), and 3 g trioctyl-phosphine oxide were mixed into a 25 mL flask and heated to 150 °C under Ar flow. At this point, the flask was moved to vacuum for 1 hour and then went back to Ar flow. The solution was heated to 370 °C for the complexion of Cd with ODPA, resulting in a colorless solution, at which point 1.5 g trioctylphosphine (TOP) was injected. The heating mantle was removed when the temperature recovered to 370 °C, letting the gradual temperature drop. At 320 °C, 0.418 g TOP:Se (0.36 g TOP and 0.058 g selenium) was swiftly injected. After the solution temperature decreased below

110 °C, toluene was injected to stop the reaction. Anhydrous toluene and methanol were adopted to purify the seeds several times. Finally, the seeds were stored in toluene.

Synthesis protocol of CdSe@CdS nanorod (SR):[27,31] 207 mg CdO (99.99%, Aldrich), 3.35 g TOPO (99%, Aldrich), 60 mg propyl phosphonic acid (PPA), 0.96 g ODPA were mixed into 25 mL flask and heated to 120 °C under vacuum for 0.5 hours. Under Ar flow, the solution was heated to 320 °C to get colorless status and went back to 120 °C and vacuumed for 2 hours. Afterward, increase the solution temperature to 340 °C, at which point 1.5 g TOP was injected. When the temperature recovered to 340 °C, 0.65 g TOP: S (ratio: 1.2 g sulfur: 15 g TOP) was rapidly injected and set the temperature to 350 °C, 2 seconds later, swiftly inject TOP:CdSe seed and keep for 15 min. The product was purified by toluene, hexane, nonanoic acid, octylamine, methanol and isopropanol (IPA), and stored in toluene.

Colloidal platinum deposition on the tip of SR:[27,53] About 5 mg CdSe@CdS nanorod was dispersed into 200 uL $Pt(AcAc)_2$/ dichlorobenzene solution (30 mg/mL). 10 mL diphenyl ether, 0.2 mL oleylamine, 0.2 mL oleic acid, and 50 mg 1,2-hexadecanediol were mixed into 25 mL three-neck flask and heated to 80 °C under vacuum for 30 min to remove the water trace. The solution went back to Ar flow and was heated to 210 °C. At this point, SR solution with $Pt(AcAc)_2$ was swiftly injected, and the solution was kept for 5 min. The sample was purified by anhydrous toluene, methanol, and IPA, and stored in toluene.

Colloidal nickel particle growth on the tip of CdSe@CdS nanorods: About 14.25 mg CdSe@CdS nanorod (42 nm length) was dispersed in 3 mL TOP; 0.16 g $Ni(AcAc)_2$ was dissolved into 3 mL TOP; then mix these two solutions and heat to 180 °C under Ar and keep for 20 min, quench to 100 °C and inject 10 mL toluene, use ethanol, methanol, isopropanol and toluene to purify the final product.

Experimental Setup and Procedure for C–O Cross-Coupling

For the setup of cross coupling experiments, the light intensity of LED (M455L4, Thorlabs, Inc.) with 455 nm is tuned by the LED driver (LEDD1B, Thorlabs, Inc.). The glass vial with reaction solution is placed into holder (CVH100, Thorlabs, Inc.). During illumination, the holder with a glass vial was covered by aluminum foil to prevent any light leak, as shown in the photograph.

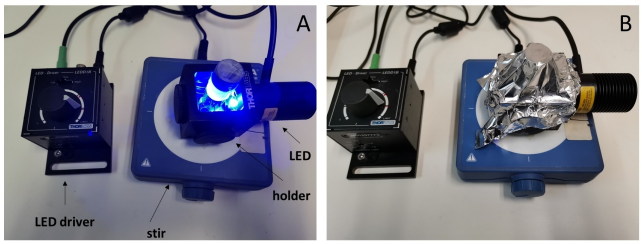

0.1 mmol methyl 4-bromobenzoate, 0.15 mmol Boc-Pro-OH, 0.03 mmol $NiCl_2 \cdot DME$, 0.045 mmol 4,4′-Di-tert-butyl-2,2′-bipyridine (dtbbpy), 0.15 mmol Cs_2CO_3 were weighed into 7 mL flamed-dried vial in glovebox filled with N_2. Stir bar, 2 mL DMF, and 0.2 mL SR toluene solution (40 nm length, 4.3 nm width, 21.29 mM Cd^{2+} concentration) were then added to the glovebox. The mixture solution was sonicated for a few seconds, and the vial was sealed with Parafilm and placed in a holder (CVH100, Thorlabs, Inc.) with 300 mW 455 nm LED. After 9 hours of illumination, 20 mL water and 10 mL methyl tert-butyl ether (MTBE) were used to extract the organic product to the MTBE part. After the second extraction was done, the 20 mL MTBE solution was dried over Na_2SO_4, and 0.1 mmol 1,3,5-trimethoxybenzene was added as an internal standard to calculate the yield (in this work, all the yields were calculated as NMR yields). For the cycle experiments, after one cycle, the SR was separated via centrifugation and then used for the next cycle. Except for DMF, no other solvent was adopted for C–O product collection and purification since the C–O cross-coupling performance of SR is very sensitive to the collection or purification process. Most products were purified by the fluorescence plate (PLC, preparative layer chromatography, Silica gel 60 F254 (0.5 mm thickness), Merck KGaA, 64271 Darmstadt, Germany) using Hexane, Dichloromethane, ethyl acetate as elution. The detailed ratio for each product was elaborated in the NMR spectra part. All the ^{1}H NMR and 13 C NMR spectra were calibrated by TMS signal at 0 ppm, C signal of chloroform-D at 77.16 ppm, respectively.

Characterizations

Optical characterization: UV-Vis absorption spectroscopy was performed by an Agilent Cary 5000 UV-Vis-NIR spectrophotometer, using standard 10 mm fluorometer cuvettes. Spectra were analyzed via the accompanying Cary WinUV software package. Photoluminescence (PL) measurements were done using a Jobin Yvon (Fluorolog-3) Fluorometer. Samples were excited at around 455 nm, and the resulting spectra were measured from 485–700 nm. The relative PL Quantum Yield (PL-QY) was determined using Rhodamine 6G (R6G) ethanol solution as reference (known QY of 95%). Lifetime measurement is performed by Edinburgh Instrument LifeSpec II with EPL-405 laser.

X-Ray diffraction (XRD) was carried out with a Rigaku Smartlab X-ray diffractometer using Cu Ka radiation (wavelength, 0.154 nm) with a slit of 2 mm.

Electron microscopy: Transmission electron microscopy (TEM) images were taken with FEI Tecnai G^2 T20 S-Twin TEM under 200 KeV. High angle angular dark-field scanning transmission electron microscopy (HAADF-STEM) images, energy-dispersive X-ray (EDX) mapping and electron energy loss spectroscopy (EELS) were recorded at an accelerating voltage of 200 keV in a double (probe and image) aberration-corrected FEI Titan Cubed Themis G^2 60–300 microscope with a semi-convergence angle of 21.7 mrad and a probe current of 0.250 nA, equipped with Dual-X detector (Bruker) and dual energy-filtered EELS detector.

NMR and MS TLC: ^{1}H and ^{13}C NMR spectra were collected on a 400 MHz Bruker Advance spectrometer with $CDCl_3$ as deuterated solvent. Thin-layer chromatography (TLC) was performed on Silicycle 0.25 mm silica gel F-254 plates. Visualization of the developed chromatogram was performed by 365 nm UV fluorescence quenching. Data for ^{1}H NMR are reported as follows: chemical shift (δ ppm), multiplicity (s = singlet, d = doublet, t = triplet, q = quartet, m = multiplet, dd = doublet of doublets, dt = doublet of triplet, ddd = doublet of doublets of doublets), coupling constants (Hz), and integration. High-resolution Electrospray ionization (ESI) mass spectra (MS) was adopted to analyze the mass of complexes via maXis Impact™ Mass Spectrometer (Bruker).

Acknowledgment

This research was carried out in the framework of the Russell Berrie Nanotechnology Institute (RBNI) and the Nancy and Stephen Grand Technion Energy Program (GTEP). The project received funding from the European Union's Horizon 2020 research and innovation programme under the Marie Skłodowska-Curie grant agreement No. 722591, and the Israeli Ministry of National Infrastructures, Energy and Water Resources (grant

number 218-11-044). The authors thank Hugo Morren (Dr Reddy's) for valuable analytical discussions, Junhong Chen, Dr. Hang Zhang, and Prof. Charles E. Diesendruck for assistance with products isolation.

Conflict of Interest

The authors declare no conflict of interest.

Data Availability Statement

The data that support the findings of this study are available in the supplementary material of this article.

Keywords: colloidal nanocrystals · cross-coupling · heterogeneous catalysis · nickel complex · photocatalysis

[1] J. Magano, J. R. Dunetz, *Chem. Rev.* **2011**, *111*, 2177–2250.
[2] R. F. Heck, J. P. Nolley, *J. Org. Chem.* **1972**, *37*, 2320–2322.
[3] E. Negishi, A. O. King, N. Okukado, *J. Org. Chem.* **1977**, *42*, 1821–1823.
[4] N. Miyaura, A. Suzuki, *J. Chem. Soc., Chem. Commun.* **1979**, *19*, 866–867.
[5] A. R. Muci, S. L. Buchwald in *Practical Palladium Catalysts for C–N and C–O Bond Formation, Vol.* (Ed. N. Miyaura), Springer Berlin Heidelberg, Berlin, Heidelberg, **2002**, pp. 131–209.
[6] J. Louie, J. F. Hartwig, *Tetrahedron Lett.* **1995**, *36*, 3609–3612.
[7] A. S. Guram, R. A. Rennels, S. L. Buchwald, *Angew. Chem. Int. Ed. Engl.* **1995**, *34*, 1348–1350.
[8] C. C. C. Johansson Seechurn, M. O. Kitching, T. J. Colacot, V. Snieckus, *Angew. Chem. Int. Ed.* **2012**, *51*, 5062–5085; *Angew. Chem.* **2012**, *124*, 5150–5174.
[9] C. Zhu, H. Yue, J. Jia, M. Rueping, *Angew. Chem.* **2021**, *133*, 17954–17975.
[10] J. A. Terrett, J. D. Cuthbertson, V. W. Shurtleff, D. W. C. MacMillan, *Nature* **2015**, *524*, 330–334.
[11] J. C. Tellis, D. N. Primer, G. A. Molander, *Science* **2014**, *345*, 433.
[12] Z. Zuo, T. Ahneman Derek, L. Chu, A. Terrett Jack, G. Doyle Abigail, W. C. MacMillan David, *Science* **2014**, *345*, 437–440.
[13] R. Welin Eric, C. Le, M. Arias-Rotondo Daniela, K. McCusker James, W. C. MacMillan David, *Science* **2017**, *355*, 380–385.
[14] L. Tian, N. A. Till, B. Kudisch, D. W. C. MacMillan, G. D. Scholes, *J. Am. Chem. Soc.* **2020**, *142*, 4555–4559.
[15] B. Pieber, J. A. Malik, C. Cavedon, S. Gisbertz, A. Savateev, D. Cruz, T. Heil, G. Zhang, P. H. Seeberger, *Angew. Chem. Int. Ed.* **2019**, *58*, 9575–9580; *Angew. Chem.* **2019**, *131*, 9676–9681.
[16] S. Gisbertz, B. Pieber, *ChemPhotoChem* **2020**, *4*, 456–475.
[17] J.-Y. Li, Y.-H. Li, M.-Y. Qi, Q. Lin, Z.-R. Tang, Y.-J. Xu, *ACS Catal.* **2020**, *10*, 6262–6280.
[18] J. A. Caputo, L. C. Frenette, N. Zhao, K. L. Sowers, T. D. Krauss, D. J. Weix, *J. Am. Chem. Soc.* **2017**, *139*, 4250–4253.
[19] Y.-Y. Liu, D. Liang, L.-Q. Lu, W.-J. Xiao, *Chem. Commun.* **2019**, *55*, 4853–4856.
[20] Z. Zhang, C. R. Rogers, E. A. Weiss, *J. Am. Chem. Soc.* **2020**, *142*, 495–501.
[21] D. V. Talapin, R. Koeppe, S. Götzinger, A. Kornowski, J. M. Lupton, A. L. Rogach, O. Benson, J. Feldmann, H. Weller, *Nano Lett.* **2003**, *3*, 1677–1681.
[22] J. Müller, J. M. Lupton, P. G. Lagoudakis, F. Schindler, R. Koeppe, A. L. Rogach, J. Feldmann, D. V. Talapin, H. Weller, *Nano Lett.* **2005**, *5*, 2044–2049.
[23] L. Carbone, C. Nobile, M. De Giorgi, F. D. Sala, G. Morello, P. Pompa, M. Hytch, E. Snoeck, A. Fiore, I. R. Franchini, M. Nadasan, A. F. Silvestre, L. Chiodo, S. Kudera, R. Cingolani, R. Krahne, L. Manna, *Nano Lett.* **2007**, *7*, 2942–2950.
[24] D. V. Talapin, J. H. Nelson, E. V. Shevchenko, S. Aloni, B. Sadtler, A. P. Alivisatos, *Nano Lett.* **2007**, *7*, 2951–2959.
[25] L. Amirav, A. P. Alivisatos, *J. Phys. Chem. Lett.* **2010**, *1*, 1051–1054.
[26] A. Sitt, F. D. Sala, G. Menagen, U. Banin, *Nano Lett.* **2009**, *9*, 3470–3476.
[27] P. Kalisman, Y. Nakibli, L. Amirav, *Nano Lett.* **2016**, *16*, 1776–1781.
[28] A. Agosti, Y. Nakibli, L. Amirav, G. Bergamini, *Nano Energy* **2020**, *70*, 104510.
[29] H. Zhu, N. Song, H. Lv, C. L. Hill, T. Lian, *J. Am. Chem. Soc.* **2012**, *134*, 11701–11708.
[30] W. W. Yu, L. Qu, W. Guo, X. Peng, *Chem. Mater.* **2003**, *15*, 2854–2860.
[31] Y. Nakibli, L. Amirav, *Chem. Mater.* **2016**, *28*, 4524–4527.
[32] G. D. Scholes, *Adv. Funct. Mater.* **2008**, *18*, 1157–1172.
[33] M. Wächtler, P. Kalisman, L. Amirav, *J. Phys. Chem. C* **2016**, *120*, 24491–24497.
[34] K. Wu, H. Zhu, T. Lian, *Acc. Chem. Res.* **2015**, *48*, 851–859.
[35] C. Mongin, S. Garakyaraghi, N. Razgoniaeva, M. Zamkov, F. N. Castellano, *Science* **2016**, *351*, 369.
[36] S. Garakyaraghi, F. N. Castellano, *Inorg. Chem.* **2018**, *57*, 2351–2359.
[37] Y. Jiang, E. A. Weiss, *J. Am. Chem. Soc.* **2020**, *142*, 15219–15229.
[38] A. Olaya-Castro, G. D. Scholes, *Int. Rev. Phys. Chem.* **2011**, *30*, 49–77.
[39] D. M. Arias-Rotondo, J. K. McCusker, *Chem. Soc. Rev.* **2016**, *45*, 5803–5820.
[40] H. B. S. G. W. T. M. J. Frisch, G. E. Scuseria, M. A. Robb, J. R. Cheeseman, G. Scalmani, V. Barone, B. Mennucci, G. A. Petersson, H. Nakatsuji, M. Caricato, X. Li, H. P. Hratchian, A. F. Izmaylov, J. Bloino, G. Zheng,J. L. Sonnenberg, M. Hada, M. Ehara, K. Toyota, R. Fukuda, J. Hasegawa, M. Ishida, T. Nakajima, Y. Honda, O. Kitao, H. Nakai, T. Vreven, J. A. Montgomery, Jr., J. E. Peralta, F. Ogliaro, M. Bearpark, J. J. Heyd, E. Brothers, K. N. Kudin, V. N. Staroverov, T. Keith, R. Kobayashi, J. Normand, K. Raghavachari, A. Rendell, J. C. Burant, S. S. Iyengar, J. Tomasi, M. Cossi, N. Rega, J. M. Millam, M. Klene, J. E. Knox, J. B. Cross, V. Bakken, C. Adamo, J. Jaramillo, R. Gomperts, R. E. Stratmann, O. Yazyev, A. J. Austin, R. Cammi, C. Pomelli, J. W. Ochterski, R. L. Martin, K. Morokuma, V. G. Zakrzewski, G. A. Voth, P. Salvador, J. J. Dannenberg, S. Dapprich, A. D. Daniels, O. Farkas, J. B. Foresman, J. V. Ortiz, J. Cioslowski, D. J. Fox. **2013**.
[41] Y. Shao, Y. Mei, D. Sundholm, V. R. I. Kaila, *J. Chem. Theory Comput.* **2020**, *16*, 587–600.
[42] S. Hirata, M. Head-Gordon, *Chem. Phys. Lett.* **1999**, *314*, 291–299.
[43] C. Adamo, V. Barone, *J. Chem. Phys.* **1999**, *110*, 6158–6170.
[44] X. Luo, Y. Han, Z. Chen, Y. Li, G. Liang, X. Liu, T. Ding, C. Nie, M. Wang, F. N. Castellano, K. Wu, *Nat. Commun.* **2020**, *11*, 28.
[45] J. De Roo, Z. Huang, N. J. Schuster, L. S. Hamachi, D. N. Congreve, Z. Xu, P. Xia, D. A. Fishman, T. Lian, J. S. Owen, M. L. Tang, *Chem. Mater.* **2020**, *32*, 1461–1466.
[46] Z. Zhang, K. Edme, S. Lian, E. A. Weiss, *J. Am. Chem. Soc.* **2017**, *139*, 4246–4249.
[47] L. Biadala, B. Siebers, R. Gomes, Z. Hens, D. R. Yakovlev, M. Bayer, *J. Phys. Chem. C* **2014**, *118*, 22309–22316.
[48] E. B. Corcoran, M. T. Pirnot, S. Lin, S. D. Dreher, D. A. DiRocco, I. W. Davies, S. L. Buchwald, D. W. C. MacMillan, *Science* **2016**, *353*, 279–283.
[49] M. Kudisch, C. H. Lim, P. Thordarson, G. M. Miyake, *J. Am. Chem. Soc.* **2019**, *141*, 19479–19486.
[50] T. Jin, N. Uhlikova, Z. Xu, Y. Zhu, Y. Huang, E. Egap, T. Lian, *J. Chem. Phys.* **2020**, *152*, 214702.
[51] X. Luo, G. Liang, Y. Han, Y. Li, T. Ding, S. He, X. Liu, K. Wu, *J. Am. Chem. Soc.* **2020**, *142*, 11270–11278.
[52] S. Garakyaraghi, C. Mongin, D. B. Granger, J. E. Anthony, F. N. Castellano, *J. Phys. Chem. Lett.* **2017**, *8*, 1458–1463.
[53] S. E. Habas, P. Yang, T. Mokari, *J. Am. Chem. Soc.* **2008**, *130*, 3294–3295.

Manuscript received: April 7, 2022
Revised manuscript received: May 3, 2022
Accepted manuscript online: May 8, 2022
Version of record online: May 26, 2022